Journal of Materials Chemistry C

Accepted Manuscript

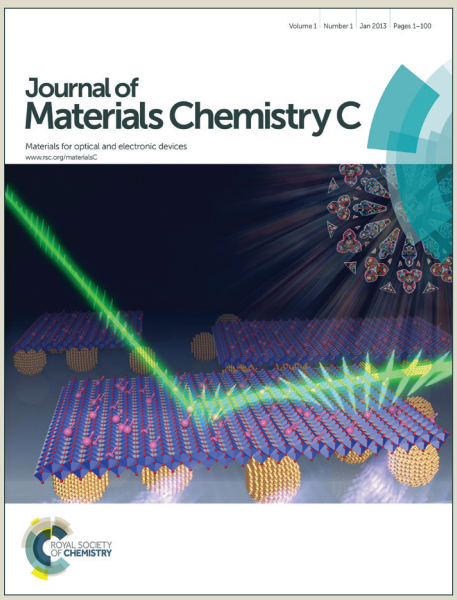

ROYAL SOCIETY OF CHEMISTRY

www.rsc.org/materialsC

Phase composition, crystal structure, infrared reflectivity and microwave dielectric properties of temperature stable composite ceramics (scheelite and zircon-type) in $BiVO_4$-YVO_4 system

Di Zhou,[*a,b] Wen-Bo Li,[a] Hai-Hong Xi,[a] Li-Xia Pang,[c] and Guang-Sheng Pang[d]

[a]Electronic Materials Research Laboratory, Key Laboratory of the Ministry of Education & International Center for Dielectric Research, Xi'an Jiaotong University, Xi'an 710049, Shaanxi, China

[b]Xi'an Jiaotong University Suzhou Academy, Suzhou 215123, Jiangsu, China

[c]Micro-optoelectronic Systems Laboratories, Xi'an Technological University, Xi'an 710032, Shaanxi, China

[d]State Key Laboratory of Inorganic Synthesis and Preparative Chemistry, Jilin University, Changchun 130021, Jilin, China

[*]Corresponding author. Tel (Fax): +86-29-82668679; E-mail address: zhoudi1220@gmail.com (Di Zhou)

Abstract

$(1-x)BiVO_4$-$xYVO_4$ ($x \leq 0.65$) ceramics were prepared by using the solid state reaction method. X-ray diffraction, Raman spectra and scanning electron microscopy techniques were employed to study the phase composition and crystal structure. The ceramic samples were composed of both monoclinic scheelite and tetragonal zircon-type phases. The best microwave dielectric properties, with a permittivity ~ 45, a Qf value 14,000 GHz and a temperature coefficient of resonant frequency (TCF) + 10 ppm/^oC, were obtained in the $0.81BiVO_4$-$0.19YVO_4$ ceramic sintered at 870 ^oC for 2 h. Far-infrared spectra study showed that Bi-O oscillations dominate microwave dielectric polarizations in the $(1-x)BiVO_4$-$xYVO_4$ ceramics. The $(1-x)BiVO_4$-$xYVO_4$ ceramics might be candidate for microwave devices application and low temperature co-fired ceramic technology (LTCC).

I. Introduction

Due to the fast development of wireless communication technology, microwave dielectric ceramics have been widely studied and used in resonator, filter, duplexer, mutiplexer, EMI (Electro Magnetic Interference) filter, patch antenna/GPS (Global Position System) antenna active module, and other microwave devices applications. Microwave dielectrics with high performance and the research on the structure-property relation have always attracted much attention.[1-3]

$BiVO_4$ ceramic was reported to possess high performance of microwave dielectric properties, with a dielectric relative permittivity ε_r ~ 68, a quality factor (Qf) ~6,500 − 8,000 GHz, a large negative temperature coefficient of resonant frequency (TCF) ~ −243 ~ −260 ppm/°C and a sintering temperature below 900 °C by Valant et al. and Wee et al.[4,5] However, the large negative TCF limited its application. In fact, the origin of its large negative TCF is a second order ferroelastic phase transition at 255 ^oC, which results in a microwave permittivity peak and causes a large positive temperature coefficient of permittivity. Formation of solid solution or composite is a popular method to modify TCF value of microwave dielectric ceramics.[6-8] In our previous work, a novel composite of monoclinic scheelite and tetragonal zircon-type solid solutions was achieved in the $(Bi_{1-x}Ce_x)VO_4$ system and a near zero TCF was obtained in the $(Bi_{0.75}Ce_{0.25})VO_4$ ceramic with a permittivity ~ 47.9, a Qf value ~ 18,000 GHz.[7] Ionic radius of eight-coordinated Ce^{3+} (1.143 Å) is a little smaller than that of Bi^{3+} (1.17 Å)[9] and a solid solubility about 10 % of Ce substitution for Bi was confirmed by X-ray diffraction analysis. Although there are some different opinions on the substitution of Ln for the Bi in scheelite monoclinic $BiVO_4$, due to the specific hybridization of the Bi 6s2 and O 2p orbitals,[10-12] it was found that the formation of

tetragonal zircon-type phase can effectively modify the TCF of $BiVO_4$ system. Here, we are inspired to use the Y^{3+} ion, with even more small ionic radius ~ 1.019 Å, to induce the formation of zircon-type solid solution. Hence, in the present work, $(1-x)BiVO_4$-$xYVO_4$ ($x \leq 0.65$) ceramics were prepared by using the solid state reaction method. Phase composition, microwave dielectric properties, and the structure-property relation were studied in detail.

II. Experimental Methods

Reagent-grade starting materials of Bi_2O_3 (> 99%, Shu-Du Powders Co. Ltd., Chengdu, China), V_2O_5 and Y_2O_3 (> 99%, Sinopharm Chemical Reagent Co., Ltd, Shanghai, China) were mixed according to the stoichiometric formulation $(Bi_{1-x}Y_x)VO_4$ ($x \leq 0.65$) (abbreviated here as BYVx), by ball milling for 4 h using a planetary mill (Nanjing Machine Factory, Nanjing, China) at 150 rpm, with the zirconia balls (2 mm in diameter) as milling media. The powder mixtures were then dried and calcined at 700 ^oC for 4 h. The calcined powders were ball milled for 5 h at 200 rpm. Then, the powders were pressed into cylinders (10 mm in diameter and 4 ~ 5 mm in height) with a steel die with 5 wt. % PVA as binder at a uniaxial pressure of 100 MPa. Samples were sintered at temperatures from 800 ^oC to 900 ^oC for 2 h.

Room temperature XRD was performed with Cu Kα radiation (Rigaku D/MAX-2400 X-ray diffractometry, Tokyo, Japan). Prior to examination, the sintered pellets were crushed in a mortar and pestle to powder. Diffraction pattern was obtained over 5 - 65 ^{o} (2θ) at a step size of 0.02 ^{o}. The results were analyzed by the Rietveld profile refinement method, using FULLPROF program. To examine grain morphology, as-fired surfaces were observed by scanning electron microscopy (SEM, FEI, Quanta 250 F). Raman spectra at room temperature were obtained on polished

pellets with a Raman spectrometer (inVia, Renishaw, England), excited by an Ar^+ laser (514.5 nm). Room temperature infrared reflectivity spectra were measured using a Bruker IFS 66v FT-IR spectrometer on the Infrared beamline station (U4) at the National Synchrotron Radiation Lab. (NSRL), China. Dielectric properties at microwave frequency were measured with the $TE_{01\delta}$ dielectric resonator method with a network analyzer (HP 8720 Network Analyzer, Hewlett-Packard) and a temperature chamber (Delta 9023, Delta Design, Poway, CA). Temperature coefficient of resonant frequency TCF (τ_f) was calculated with the following formula:

$$TCF(\tau_f) = \frac{f_T - f_{T_0}}{f_{T_0} \times (T - T_0)} \times 10^6, \quad (1)$$

where f_T and f_{T0} are the $TE_{01\delta}$ resonant frequencies at temperature T and T_0, respectively.

III Results and Discussions

XRD patterns of the (1-x)$BiVO_4$-xYVO_4 ($x \leq 0.65$) samples calcined at 700 ^oC for 4 h and sintered at different temperatures are shown in Fig. 1. As seen from all the patterns of calcined samples, both peaks of scheelite monoclinic and zircon-type tetragonal phases can be observed. Large difference between the ionic radii of Bi^{3+} and Y^{3+} (1.17 Å and 1.019 Å, respectively) determines that Y^{3+} can not enter the A site of monoclinic scheelite but rearranged with the VO_4 tetrahedrons and formed the zircon-type structured phase YVO_4. This is different from the situation in the $(Bi_{1-x}Ce_x)VO_4$ systems,[7] in which the monoclinic solid solution could be formed within $x \leq 0.10$. For the calcined samples as shown in Fig. 1 (a), intensity of the zircon-type tetragonal phase increased continuously with increasing x value meanwhile the intensity of monoclinic scheelite phase decreased. For BYV0.65

sample, main peaks of the monoclinic scheelite phase can hardly be observed. XRD results for the sintered samples are a little different from that of calcined samples. It can be observed in both BYV0.19 and BYV0.25 samples that main peak of the scheelite phase is stronger than that of the zircon-type phase in the calicined samples while it is opposite in the sintered ones. It is obvious that content of zircon-type tetragonal phase is higher in sintered samples than that in calcined samples. This result gives a conclusion that phase equilibrium in the (1-x)$BiVO_4$-xYVO_4 ($x \leq 0.65$) ceramic can be influenced by the temperature. Furthermore, solid solubility of Bi^{3+} in zircon-type $(Bi_{1-x}Y_x)VO_4$ phase reached 60 % at a sintering temperature 850 ^oC. To evaluate the concentrations of different phases, content ratio of the zircon-type phase was calculated approximately using the following equation:

Content of zircon-type phase=$I_{z(2\,0\,0)}/ (I_{z(2\,0\,0)}+ I_{s(1\,1\,2)})$, (2)

Ration of zircon-type phase as a function of x value in both calcined and sintered samples are presented in Fig. 1 (c). It is seen that high temperatures can effectively enhance the zircon-type content in (1-x)$BiVO_4$-xYVO_4 ceramics within $0.0 < x \leq 0.65$.

The refinements were performed using Fullprof software based on X-ray diffraction data of the 0.82$BiVO_4$-0.19YVO_4 and $(Bi_{0.35}Y_{0.65})VO_4$ samples. The observed and calculated XRD patterns are shown in Fig. 2 (a) and (b). The refined lattice parameters for monoclinic scheelite and zircon-type phases ($BiVO_4$ and $(Bi_{0.6}Y_{0.4})VO_4$ compositions were supposed) in the 0.82$BiVO_4$-0.19YVO_4 sample are a = 5.176(5) Å, b = 5.096(6) Å, c = 11.675(5) Å, γ = 90.23(3) ° with a space group I 1 1 2/b (15) according to the data (ICSD #100602) reported by Sleight et al.[13] and $a = b$ = 7.255(4) Å, c = 6.418(6) Å with a space group I 4_1/amd (141) according to the data (ICSD #100733) reported by Dreyer et al.,[14] respectively. Amount of the zircon-type

phase is about 59.15 %, which is similar to the result calculated from Equ. 2. The refined values of lattice parameters for the $(Bi_{0.35}Y_{0.65})VO_4$ sample are $a = b = 7.175(8)$ Å, $c = 6.347(7)$ Å, with a space group I 4_1/amd (141). All the atomic fractional coordinates and structure details are listed in Table I, II and III. V-O distance in the zircon-type $(Bi_{0.35}Y_{0.65})VO_4$ sample is 1.6975 Å, which is a little smaller than that in YVO_4 (1.7058 Å). The distances of the long and short (Bi,Y)-O bonds are 2.3371 Å and 2.4631 Å, respectively, which are larger than that in YVO_4 (2.2986 Å and 2.4434 Å, respectively),[15] and this can be attributed to the larger ionic radius of Bi^{3+} than Y^{3+}.

To study cell parameters change trends of the ABO_4 (B = V^{5+}; A= Sc^{3+}, Ln^{3+}, Bi^{3+}) type compounds, Fig. 3 presents the *a*, *b*, *c*, cell volume, A-O bond length, and V-O bond length as a function of ionic radius of A site using data from literatures and this work.[14-18] It can be seen that as A site ionic radius increases from 0.87 Å (for Sc^{3+}) to 1.16 Å (for La^{3+}), both the $a = b$ and *c* parameters increase almost linearly and this results in the linear increase of cell volume ($= a \times b \times c$). As seen from the schematic crystal structure in Fig. 1 (d), there are two A ions (or two AO_8 dodecahedra) observed along all the *a*, *b*, and *c* axes and this can explain the linear increase of cell parameters. When ionic radius increases to 1.17 Å for Bi^{3+}, *a* (= *b*) parameter decreases while *c* increases slightly and this results in the slight decrease of cell volume. It seems that 1.17 Å (for Bi^{3+}) of A site ionic radius is a limit for the zircon-type tetragonal structure. In fact, the zircon-type $BiVO_4$ can only be synthesized by the wet chemical method and it can irreversibly transform into the monoclinic scheelite phase when heated above 400 ^oC.[19,20] However, the zircon-type structured $(Bi_{0.35}Y_{0.65})VO_4$ ceramic is quite stable. Cell parameters of the $(Bi_{0.35}Y_{0.65})VO_4$ lie between that of YVO_4 and $BiVO_4$ and are consistent with the linear relation (Vegard's law). As show in Fig. 3 (b), there are two different types of A-O bonds when the A site ionic radius is

≤ 1.109 Å (for Nd^{3+}). Both of them first increased linearly with increasing A site ionic radius and then became equal to each other (with the sudden drop of the long one) when A site ion is ≥ 1.126 Å (for Pr^{3+}). When A site is occupied by Bi, the Bi-O bond length decreased a little and this corresponds with the decrease of *a* and *b* parameters. The V-O bond length (or the VO_4 tetrahedron) seems to be independent on the A site ionic radius and keeps stable at around 1.7 Å. This implies that the zircon-type structure is spacious enough and VO_4 tetrahedron volumes can not be influenced by increasing AO_8 dodecahedra volumes.

Figure 4 shows room-temperature Raman spectra of the (1-x)$BiVO_4$-xYVO_4 ceramics (x = 0.10, 0.15, 0.175, 0.25, 0.40 and 0.65) over 100 ~ 1150 cm^{-1}. For 0.9$BiVO_4$-0.1YVO_4 ceramic, Raman bands at 825.7 cm^{-1} and the weak shoulder at about 715.6 cm^{-1} are assigned to ν_s(V–O) (the symmetric V-O stretching mode, A_g symmetry) and ν_{as}(V–O) (the anti-symmetric V-O stretching mode, B_g symmetry), respectively. The bands at 365.0 and 332.2 cm^{-1} are assigned to the $\delta_s(VO_4^{3-})$ and $\delta_{as}(VO_4^{3-})$, respectively (the symmetric A_g bending mode of vanadate anion and the anti-symmetric B_g bending mode of vanadate anion). The bands below 300 cm^{-1} belong to the external modes (rotation/translation).[21-23] With the increase of x value, intensity of the characteristic band of zircon-type phase at 879 cm^{-1} (A_{1g}, ν_1) became stronger and stronger. Generally, two sets of Raman spectra could be observed when x < 0.65 and this agrees well with the result from the X-ray analysis. For $(Bi_{0.35}Y_{0.65})VO_4$ ceramic, the band at 802.3 cm^{-1} is assigned to the B_{2g} (ν_3). The bands at 373.7 cm^{-1} and 479.9 cm^{-1} are assigned to the A_{1g} (ν_2) and B_{2g} (ν_4), respectively. All the results correspond well with the literatures' reports.[24-27] The empirical relations[28] (ν=21349*exp(-1.9176R), where ν is the Raman shift in cm^{-1} and R is the V-O bond length in Å) have been found between the metal–oxygen Raman stretching

frequencies and bond lengths for vanadium and the shorter distance of V–O in zircon-type phase than that in scheelite phase can explain the blue-shift of ν_s(V–O) mode. The calculated V-O bond length in $(Bi_{0.35}Y_{0.65})VO_4$ is 1.6635 Å (using the ν_1= 879 cm^{-1}), which is similar to the result (1.6975 Å) obtained from the XRD refinement.

Microwave dielectric properties of the (1-x)$BiVO_4$-xYVO_4 ceramics as a function of x value are shown in Fig. 5. YVO_4 single crystal was reported to possess a permittivity ~ 9.4 and a Qf value ~ 280,000 GHz at 16.3 GHz.[29] According to the Lichtenecker empirical logarithmic rule,[30] it is understandable that the microwave dielectric permittivity decreased from 69 of $BiVO_4$ to 20.5 of $(Bi_{0.35}Y_{0.65})VO_4$ ceramic. As the increase of x value, Qf value first increased linearly from 8,500 GHz to 17,800 GHz at x = 0.15, then decreased slightly to 12,500 GHz at x = 0.25 and finally increased again slightly. Qf values are usually influenced by many aspects, such as grain boundary, defect, etc., and usually the simple linear results can not be obtained in the composites compared with the situation in the solid solution. TCF value increased from - 260 ppm/^oC for pure $BiVO_4$ to + 80 ppm/^oC at x = 0.25 and then decreased slightly to + 32 ppm/^oC at x = 0.65. It is quite sure that TCF value was influenced seriously by permittivity in the $(Bi_{1-x}Y_x)VO_4$ zircon-type solid solution. The best microwave dielectric properties with a permittivity ~ 45, a Qf value 14,000 GHz and a TCF value + 10 ppm/^oC were obtained in the 0.81$BiVO_4$-0.19YVO_4 ceramic sintered at 875 ^oC for 2 h. SEM image of 0.81$BiVO_4$-0.19YVO_4 ceramic sintered at 875 ^oC is shown in the insert. Due to similar composition of the scheelite and zircon-type solid solutions, it is difficult to distinguish them from the back scattered electron image. However, it is clear that there are two different types of grains with different grain sizes, 1 μm and 2.5 ~ 5 μm, respectively. The big grains

belong to the $BiVO_4$ scheelite phase and its grain size is a little smaller than that of $BiVO_4$ ceramic sintered at 840 ^oC for 2 as reported in our previous work, which means that the existence of zircon-type phase restrained the grain growth of $BiVO_4$ phase. The small grains belong to the $(Bi_{0.4}Y_{0.6})VO_4$ zircon-type phase and it seems that the existence of $BiVO_4$ effectively lowered the sintering temperature.

Microwave dielectric permittivity and Qf value as a function of temperature in the range 25 ~ 130 ^oC are shown in Fig. 6. It is seen that microwave dielectric permittivity increased with temperature when $x \leq 0.175$, which means that the temperature coefficient of permittivity is positive. When x value is ≥ 019, microwave dielectric permittivity was found to decrease slightly with temperature. Take the BYV0.19 sample for example, its permittivity decreased slightly from 44.99 at room temperature to 44.94 at 135 ^oC, which means that it is quite stable in wide temperature range and suitable for communication device application. Almost all the Qf value of $(1-x)BiVO_4$-$xYVO_4$ ceramics decreased linearly with temperature, which means the dielectric loss increased with temperature.

To further study intrinsic microwave dielectric properties, IR reflectivity spectra of the $(1-x)BiVO_4$-$xYVO_4$ ceramics were analyzed by using a classical harmonic oscillator model as follows:[31,32]

$$\varepsilon^*(\omega) = \varepsilon_\infty + \sum_{j=1}^{n} \frac{\omega_{pj}^2}{\omega_{oj}^2 - \omega^2 - j\gamma_j\omega}, \quad (3)$$

where $\varepsilon^*(\omega)$ is complex dielectric function, ε_∞ is the dielectric constant caused by the electronic polarization at high frequencies, γ_j, ω_{oj}, and ω_{pj} are the damping factor, the transverse frequency, and plasma frequency of the j-th Lorentz oscillator, respectively, and n is the number of transverse phonon modes. The complex reflectivity $R(\omega)$ can be written as:

$$R(\omega) = \left| \frac{1 - \sqrt{\varepsilon^*(\omega)}}{1 + \sqrt{\varepsilon^*(\omega)}} \right|^2, \quad (4)$$

Fitted IR reflectivity values are shown in Fig. 7, and complex permittivities are shown in Fig. 8. For all the spectra, bands at 600 – 1000 cm^{-1} can be assigned to $\nu_1(VO_4)$ and $\nu_3(VO_4)$ and the bands at 200 – 600 cm^{-1} can be assigned to $\nu_2(VO_4)$ and $\nu_4(VO_4)$ while the bands below 200 cm^{-1} can be assigned to the Bi–O band.[33-36] Spectra of the $0.9BiVO_4$-$0.1YVO_4$ and $(Bi_{0.35}Y_{0.65})VO_4$ samples are similar to the literatures' reports. It is seen that the reflectivity intensities of bands below 300 cm^{-1} become weaker while the bands above 600 cm^{-1} become stronger with the increase of x value. All the calculated dielectric permittivity and dielectric loss values are almost equal to the measured ones using $TE_{01\delta}$ method, which implies that majority of the dielectric contribution for this system at microwave region was attributed to the absorptions of phonon oscillation at infrared region and very little contribution from defect phonon scattering. Fig. 9 presents the distribution diagram of dielectric permittivity contribution and measured values as a function of x value. It is seen that dielectric contributions from the infrared bands above 200 cm^{-1} (including optical values) differs a little with composition and the change trend of microwave permittivity is dominated by the far-infrared bands with wave-number below 200 cm^{-1}, which implies that the Bi-O oscillations dominate microwave dielectric polarizations of the $(1-x)BiVO_4$-$xYVO_4$ ceramics. This can also be explained by the largest ionic polarization of Bi^{3+} (6.12 $Å^3$) among all the cations (2.92 $Å^3$ for V^{5+} and 3.81 $Å^3$ for Y^{3+}),[37] which is similar to our previous work.[38]

IV. Conclusions

The $(1-x)BiVO_4$-$xYVO_4$ ceramics were found to be composed of both monoclinic

scheelite $BiVO_4$ and tetragonal zircon-type $(Bi_{0.6}Y_{0.4})VO_4$ phases. There is no evidence that Y can enter the A site of scheelite $BiVO_4$. It is found that the high temperature can effectively accelerate the formation of zircon-type phase in the $(1-x)BiVO_4$-$xYVO_4$ ceramics ($0.10 \leq x \leq 0.65$) and the concentration of zircon-type tetragonal phase is higher than that in the calcined samples. TCF value can be easily modified by adjusting the x value and the best microwave dielectric properties with a permittivity ~ 45, a Qf value 14,000 GHz and a TCF value + 10 ppm/^oC were obtained in the $0.81BiVO_4$-$0.19YVO_4$ ceramic sintered at 870 ^oC for 2 h. The $(1-x)BiVO_4$-$xYVO_4$ ceramics might be candidate for the microwave devices application.

Acknowledgements

This work was supported by National Natural Science Foundation of China (51202182, 51202178), National Key Scientific Instrument and Equipment Development Project (2011YQ130018), the Fundamental Research Funds for the Central University, the international cooperation project of Shaanxi Province (2013KW12-04), the State Key Laboratory of Inorganic Synthesis and Preparative Chemistry (Jilin University, 2014-08) and the 111 Project of China (B14040). The author would like to thank the administrators in IR beamline workstation of National Synchrotron Radiation Laboratory (NSRL) for their help in the IR measurement. The SEM work was done at International Center for Dielectric Research (ICDR), Xi'an Jiaotong University, Xi'an, China and the authors thank Ms. Yan-Zhu Dai for her help in using SEM.

References

1 I. M. Reaney, D. Iddles, *J. Am. Ceram. Soc.*, 2006, **89**, 2063.

2 M. T. Sebastian, H. Jantunen, *Int. Mater. Rev.*, 2008, **53**, 57.

3 H. Kagata, T. Inoue, J. Kato, I. Kameyama, *Jpn. J. Appl. Phys.*, 1992, **31**, 3152.

4 M. Valant, D. Suvorov, *J. Am. Ceram. Soc.*, 2000, **83**, 2721.

5 S. H. Wee, D. W. Kim, S. I. Yoo, *J. Am. Ceram. Soc.*, 2004, **87**, 871.

6 D. Zhou, L. X. Pang, J. Guo, Z. M. Qi, T. Shao, X. Yao, C. A. Randall, *J. Mater. Chem.*, 2012, **22**, 21412.

7 D. Zhou, L. X. Pang, J. Guo, Z. M. Qi, T. Shao, Q. P. Wang, H. D. Xie, X. Yao, C. A. Randall, *Inorg. Chem.*, 2014, **53**, 1048.

8 M. Valant, D. Suvorov, C. Hoffmann, H. Sommariva, *J. Eur. Ceram. Soc.*, 2001, **21**, 2647.

9 R. D. Shannon, *Acta Cryst.*, 1976, **A32**, 751.

10 M. Dragomir, I. Arcon, S. Gardonio, M. Valant, *Acta Mater.*, 2013, **61**, 1126.

11 D. J. Payne, M. Robinson, R. G. Egdell, A. Walsh, J. McNulty, K. E. Smith, L. F. J. Piper, *Appl. Phys. Lett.*, 2011, **98**, 212110.

12 A. Walsh, Y. Yan, M. N. Huda, M. M. Al-Jassim, S. H. Wei, *Chem. Mater.*, 2009, **21**, 547.

13 A. W. Sleight, H. Y. Chen, A. Ferretti, D. E. Cox, *Mater. Res. Bull.*, 1979, **14**, 1571.

14 G. Dreyer, E. Tillmanns, *Neues Jahrb. Mineral. Monatsh.*, 1981, **4**, 151.

15 J. A. Baglio, O. J. Sovers, *J. Solid State Chem.*, 1971, **3**, 458.

16 B. C. Chakoumakos, M. M. Abraham, L. A. Boatner, *J. Solid State Chem.*, 1994, **109**, 197.

17 W. O. Milligan, L. W. Vernon, *J. Phys. Chem.*, 1952, **56**, 145.

18 Y. Oka, T. Yao, N. Yamamoto, *J. Solid State Chem.*, 2000, **152**, 486.

19 J. D. Bierlein, A. W. Sleight, *Solid State Commun.*, 1975, **16**, 69.

20 J. W. E. Mariathasan, R. M. Hazen, L. W. Finger, *Phase Transitions*, 1986, **6**, 165.

21 R. L. Frost, D. A. Henry, M. L. Weier, W. Martens, *J. Raman Spectrosc.*, 2006, **37**, 722.

22 A. Zhang, J. Zhang, N. Cui, X. Tie, Y. An, L. Li, *J. Mol. Catal. A-Chem.*, 2009, **304**, 28.

23 J. Yu, A. Kudo, *Adv. Funct. Mater.*, 2006, **16**, 2163.

24 S. A. Miller, H. H. Caspers, H. E. Rast, *Phys. Rev.*, 1968, **168**, 964.

25 R. Vali, *Solid State Commun.*, 2009, **149**, 1637.

26 G. Blasse, A. Bril, *J. Chem. Phys.*, 1968, **48**, 217.

27 G. Boulon, *J. Phys. (Paris)*, 1971, **32**, 333.

28 F. D. Hardcastle, I. E. Wachs, *J. Phys. Chem.*, 1991, **95**, 5031.

29 M. V. Jacob, J. Mazierska, J. Krupka, *J. Electroceram.*, 2005, **15**, 237.

30 Y. G. Wu, X. H. Zhao, F. Li, Z. G. Fan, *J. Electroceram.*, 2003, **11**, 227.

31 K. Wakino, M. Murata, H. Tamura, *J. Am. Ceram. Soc.*, 1986, **69**, 34.

32 S. Kamba, H. Wang, M. Berta, F. Kadlec, J. Petzelt, D. Zhou, X. Yao, X, *J. Eur. Ceram. Soc.*, 2006, **26**, 2861.

33 M. Gotic, S. Music, *J. Mol. Struct.*, 2005, **535**, 744.

34 V. P. Tolstoy, E. V. Tolstobrov, *Solid State Ionics*, 2002, **151**, 165.

35 O. Yamaguchi, Y. Mukaida, H. Shigeta, H. Takemura, M. Yamashita, *Mater. Lett.*, 1988, **7**, 1558.

36 T. Hirata, A. Watanabe, *J. Solid State Chem.*, 2001, **158**, 254.

37 R. D. Shannon, *J. Appl. Phys.*, 1993, **73**, 348.

38 D. Zhou,; W. B. Li, L. X. Pang, J. Guo, Z. M. Qi, T. Shao, X. Yao, C. A. Randall,

Dalton Trans., 2014, **43**, 7290.

Table I. Refined atomic fractional coordinates from XRD data for the $BiVO_4$ (in the $0.81BiVO_4$-$0.19YVO_4$ sample) and the lattice parameters at room temperature are a = 5.176(5) Å, b = 5.096(6) Å, c = 11.675(5) Å, γ = 90.23(3) °. The space group is I 1 1 2/b (15).

Atom	Site	Occ.	x	y	z	Biso.
Bi	4e	0.50	0.00000	0.25000	0.63213	0.66369
V	4e	0.50	0.00000	0.25000	0.12743	0.45934
O1	8f	1.00	0.15167	0.48705	0.20649	0.17135
O2	8f	1.00	0.26426	0.37973	0.44537	0.47786

Table II. Refined atomic fractional coordinates from XRD data for the $(Bi_{0.6}Y_{0.4})VO_4$ (in the $0.81BiVO_4$-$0.19YVO_4$ sample) and the lattice parameters at room temperature are $a = b = 7.255(4)$ Å, $c = 6.418(6)$ Å. The space group is I 41/amd (141).

Atom	Site	Occ.	x	y	z	Biso.
Y	4a	0.05	0.00000	0.75000	0.12500	0.09866
Bi	4a	0.075	0.00000	0.75000	0.12500	0.09866
V	4b	0.12500	0.00000	0.25000	0.37500	3.17324
O	16h	0.50000	0.00000	0.06768	0.20386	3.85294

Table III. Refined atomic fractional coordinates from XRD data for the $(Bi_{0.35}Y_{0.65})VO_4$ sample and the lattice parameters at room temperature are $a = b =$ 7.175(8) Å, c = 6.347(7) Å. The space group is I 41/amd (141).

Atom	Site	Occ.	x	y	z	Biso.
Y	4a	0.08125	0.00000	0.75000	0.12500	0.18851
Bi	4a	0.04375	0.00000	0.75000	0.12500	0.18851
V	4b	0.12500	0.00000	0.25000	0.37500	0.02877
O	16h	0.50000	0.00000	0.06809	0.20406	0.06667

Figure Captions:

Fig. 1. X-ray diffraction patterns of the (1-x)$BiVO_4$-xYVO_4 samples calcined at 700 ^oC for 4 h (a), sintered at different temperatures (b) (* - scheelite phase, o - zircon-type phase), the ration of zircon-type phase as a function of x value (c), and schematic crystal structure of zircon-type phases (d)

Fig. 2. Experimental (circles) and calculated (line) X-ray powder diffraction profiles for the 0.81$BiVO_4$-0.19YVO_4 (a) and $(Bi_{0.35}Y_{0.65})VO_4$ (b) compositions sintered at 900 ^oC for 2 h at room temperature (R_p = 13.6 %, R_{wp} = 16.6 % and R_{exp} = 12.84 % for 0.81$BiVO_4$-0.19YVO_4. R_p = 15.4 %, R_{wp} = 17.3 % and R_{exp} = 14.31 % for $(Bi_{0.35}Y_{0.65})VO_4$ The short vertical lines below the patterns mark the positions of Bragg reflections. The bottom continuous line is the difference between the observed and the calculated intensity)

Fig. 3 Cell parameters of the zircon-type ABO_4 (B = V^{5+}) type compounds as a function of the ionic radius of A site (A= Sc^{3+}, Ln^{3+}, Bi^{3+})

Fig. 4 Raman spectra of the (1-x)$BiVO_4$-xYVO_4 ceramics (x = 0.10, 0.15, 0.175, 0.25, 0.40 and 0.65)

Fig. 5 Microwave dielectric permittivity, Qf value and TCF value of the (1-x)$BiVO_4$-xYVO_4 ceramics as a function of x value and the SEM photo of BYV0.19 ceramic sintered at 875 ^oC for 2 h (S-$BiVO_4$ scheelite phase, Z-(Bi,Y)VO_4 zircon-type phase)

Fig. 6 Temperature dependence of microwave dielectric permittivity (a) and Qf value (b) of the (1-x)$BiVO_4$-xYVO_4 ceramics

Fig. 7. Measured and calculated infrared reflectivity spectra of the (1-x)$BiVO_4$-xYVO_4 ceramics (solid line for fitting values and hollow symbol for measured values)

Fig. 8. Complex dielectric spectra of the (1-x)$BiVO_4$-xYVO_4 ceramics (circles are experimental at microwave region, solid lines represent the fit of IR spectra)

Fig. 9. Distribution diagram of dielectric permittivity contribution and measured values as a function of x value in (1-x)$BiVO_4$-xYVO_4

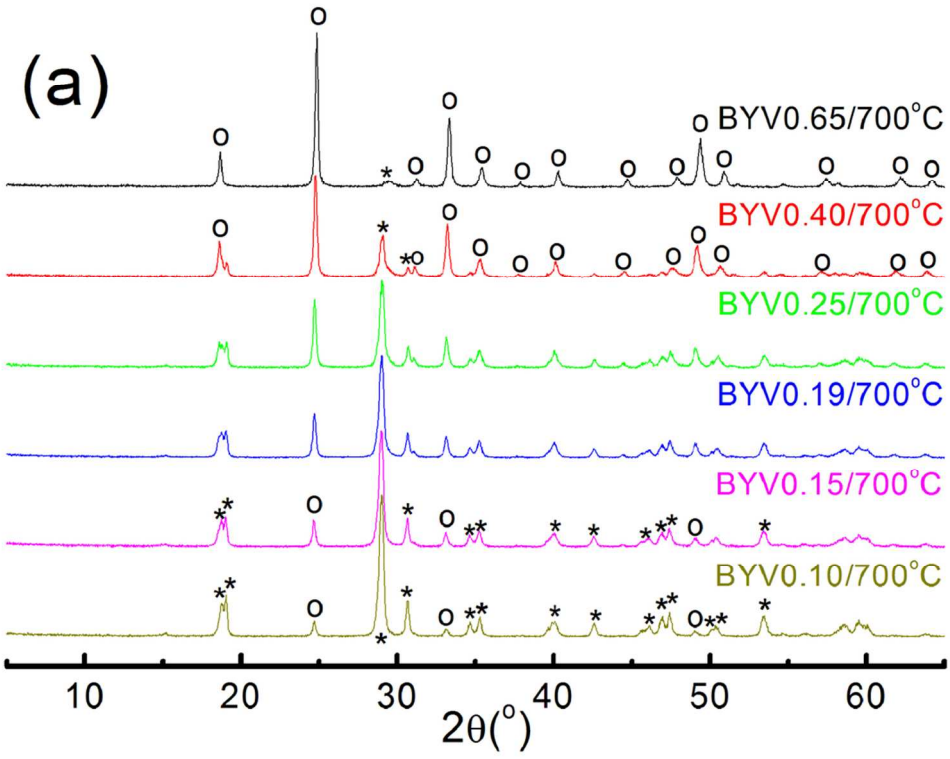

Fig. 1. X-ray diffraction patterns of the (Bi1-xYx)VO4 samples calcined at 700 oC for 4 h (a), sintered at different temperatures (b) (* - scheelite phase, o - zircon-type phase), the ration of zircon-type phase as a function of x value (c), and schematic crystal structure of zircon-type phases (d)
48x37mm (600 x 600 DPI)

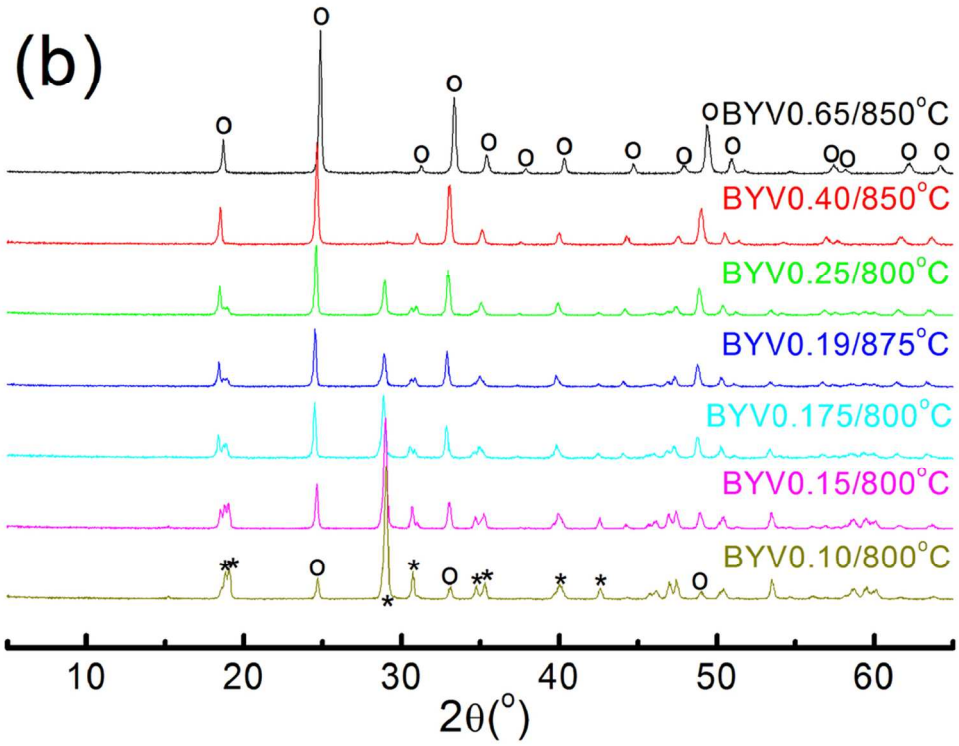

Fig. 1. X-ray diffraction patterns of the (Bi1-xYx)VO4 samples calcined at 700 oC for 4 h (a), sintered at different temperatures (b) (* - scheelite phase, o - zircon-type phase), the ration of zircon-type phase as a function of x value (c), and schematic crystal structure of zircon-type phases (d)
48x37mm (600 x 600 DPI)

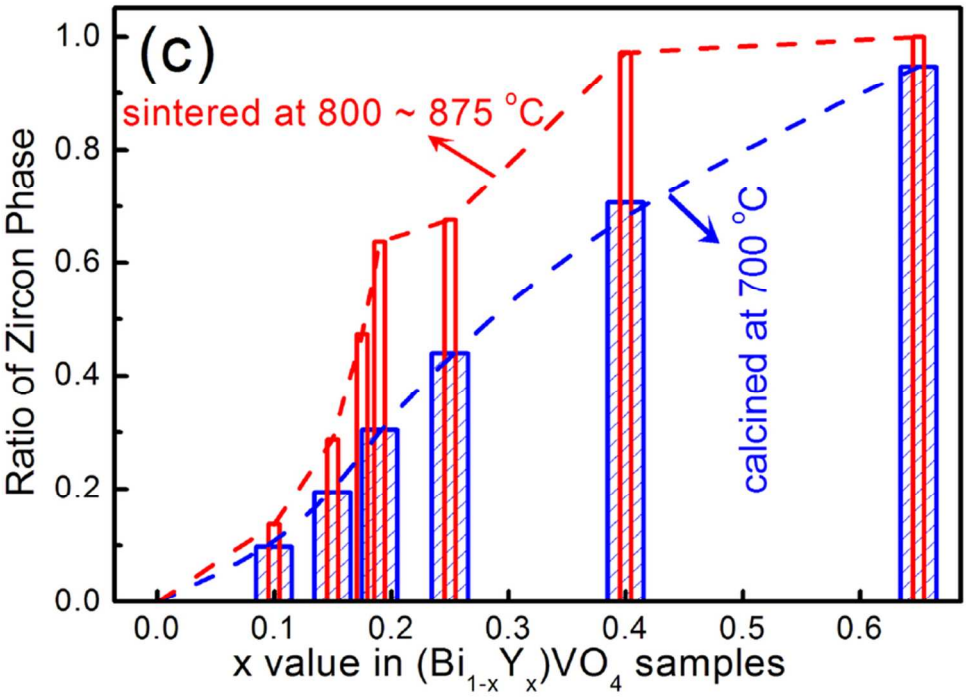

Fig. 1. X-ray diffraction patterns of the (Bi1-xYx)VO4 samples calcined at 700 oC for 4 h (a), sintered at different temperatures (b) (* - scheelite phase, o - zircon-type phase), the ration of zircon-type phase as a function of x value (c), and schematic crystal structure of zircon-type phases (d)
75x54mm (300 x 300 DPI)

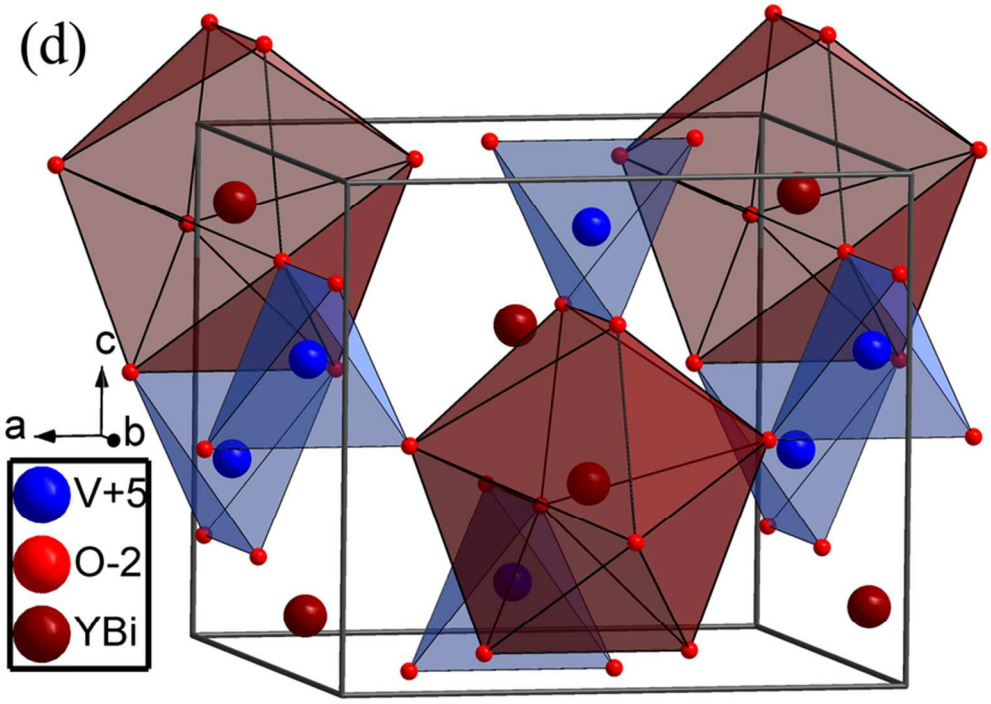

Fig. 1. X-ray diffraction patterns of the (Bi1-xYx)VO4 samples calcined at 700 oC for 4 h (a), sintered at different temperatures (b) (* - scheelite phase, o - zircon-type phase), the ration of zircon-type phase as a function of x value (c), and schematic crystal structure of zircon-type phases (d)
77x56mm (300 x 300 DPI)

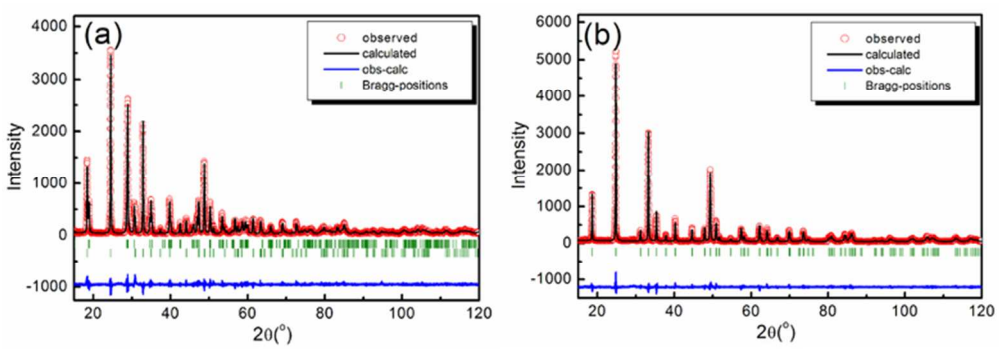

33x11mm (600 x 600 DPI)

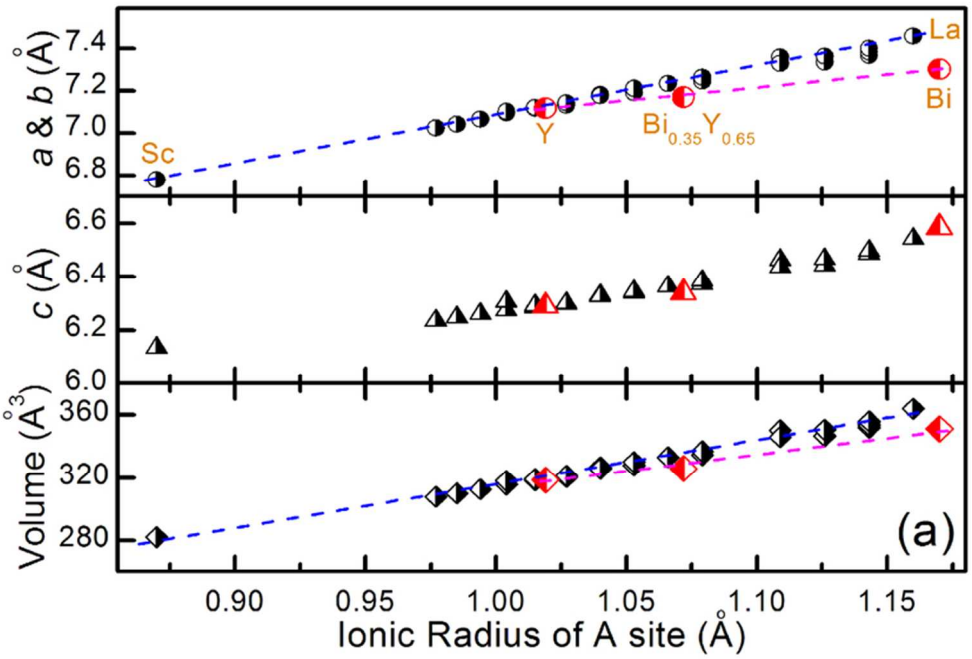

Fig. 3 Cell parameters of the zircon-type ABO4 (B = V5+) type compounds as a function of the ionic radius of A site (A= Sc3+, Ln3+, Bi3+)
72x49mm (300 x 300 DPI)

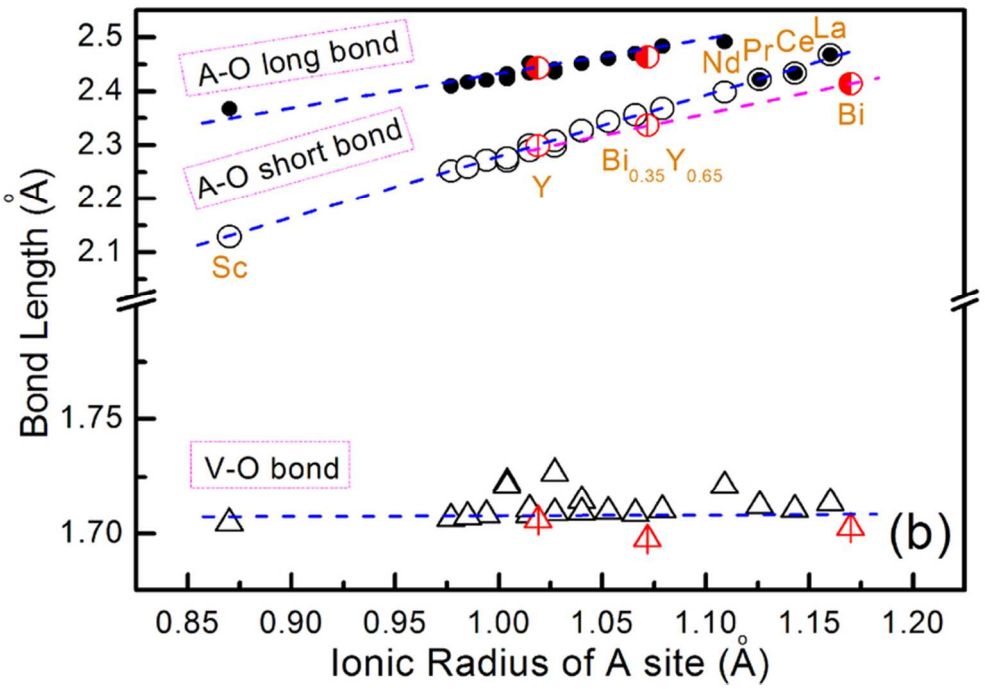

Fig. 3 Cell parameters of the zircon-type ABO4 (B = V5+) type compounds as a function of the ionic radius of A site (A= Sc3+, Ln3+, Bi3+)
72x49mm (300 x 300 DPI)

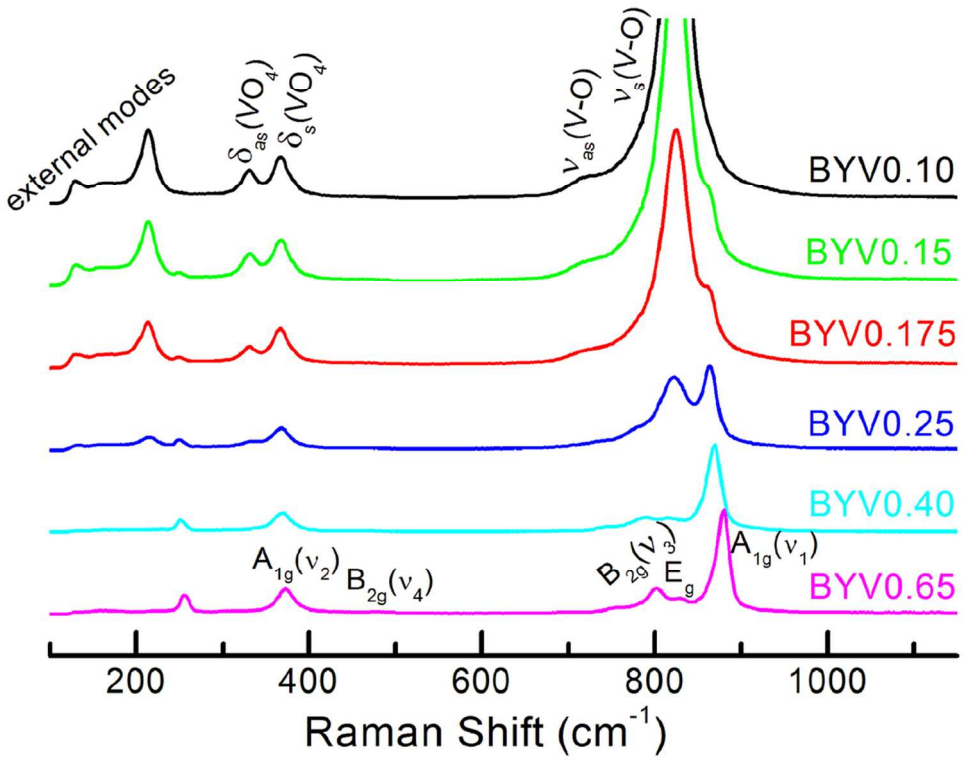

48x37mm (600 x 600 DPI)

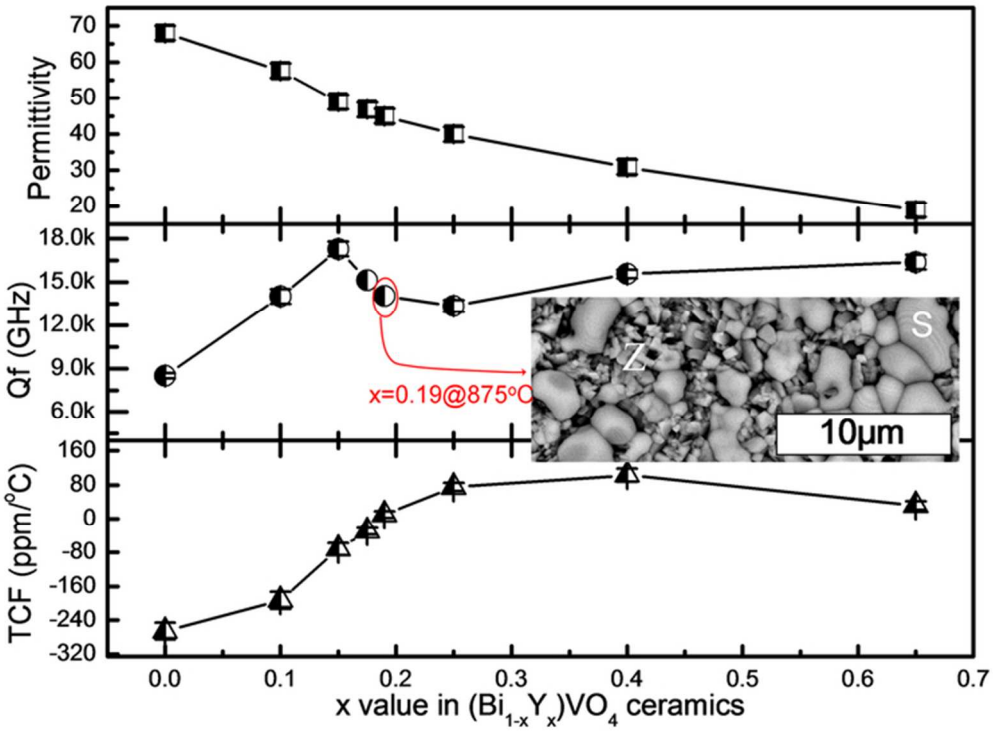

63x47mm (300 x 300 DPI)

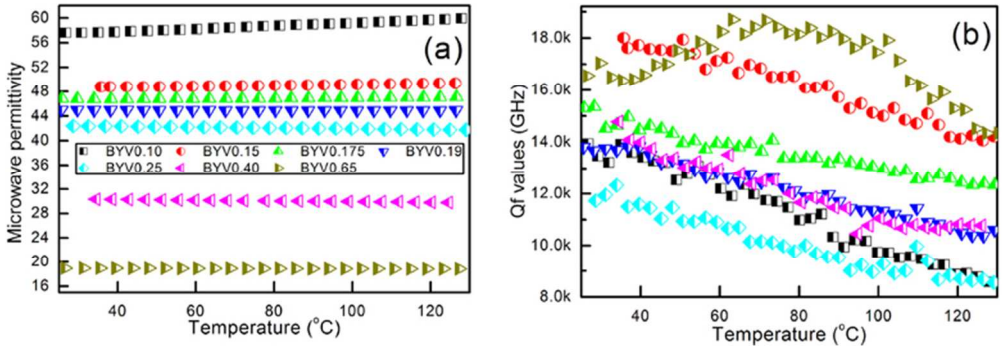

33x11mm (600 x 600 DPI)

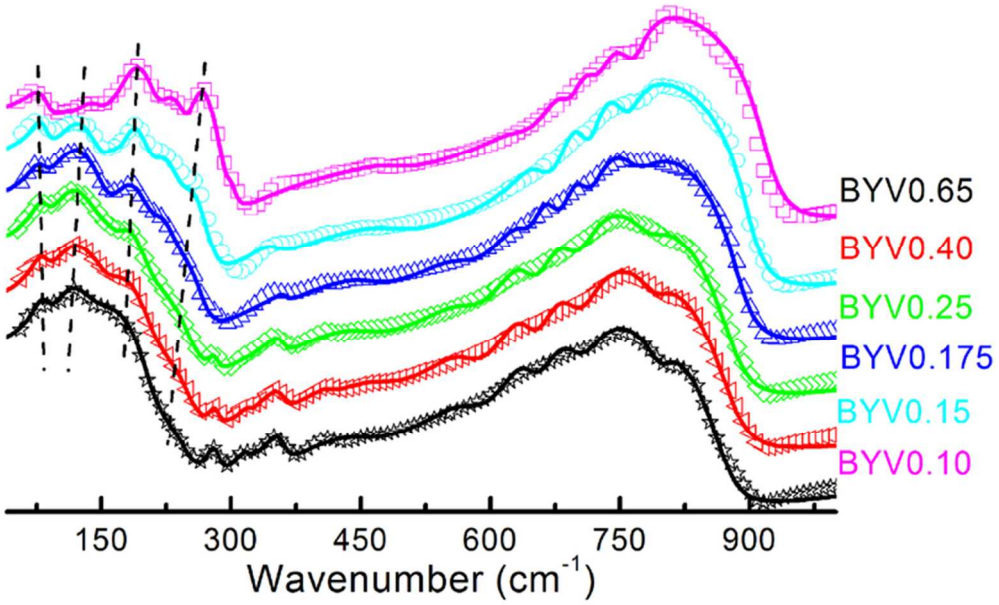

68x44mm (300 x 300 DPI)

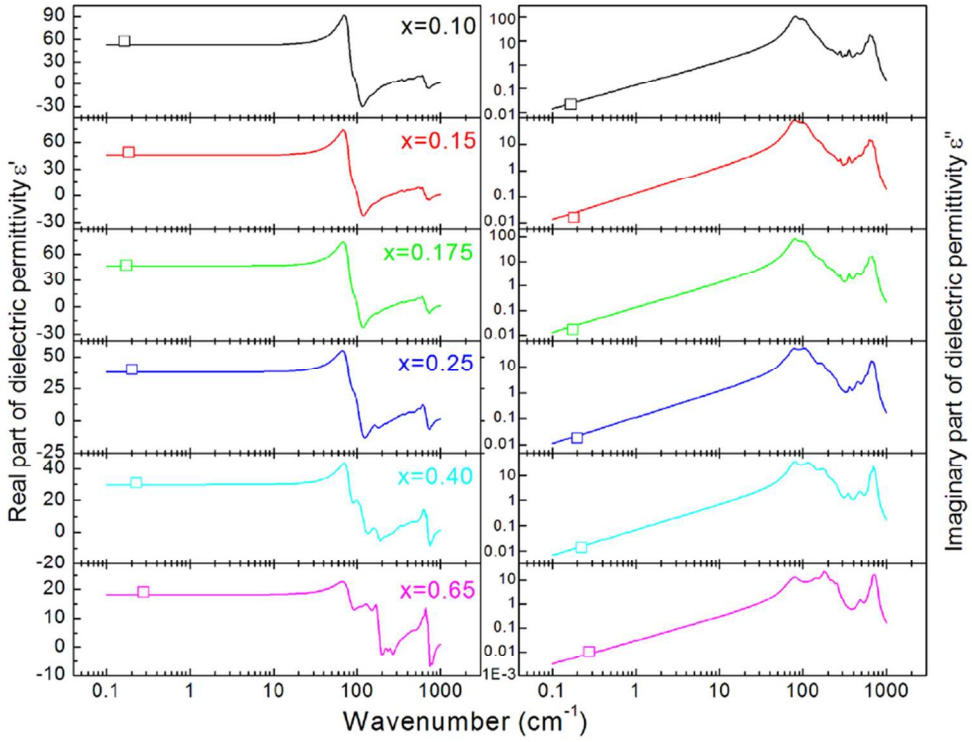

80x61mm (300 x 300 DPI)

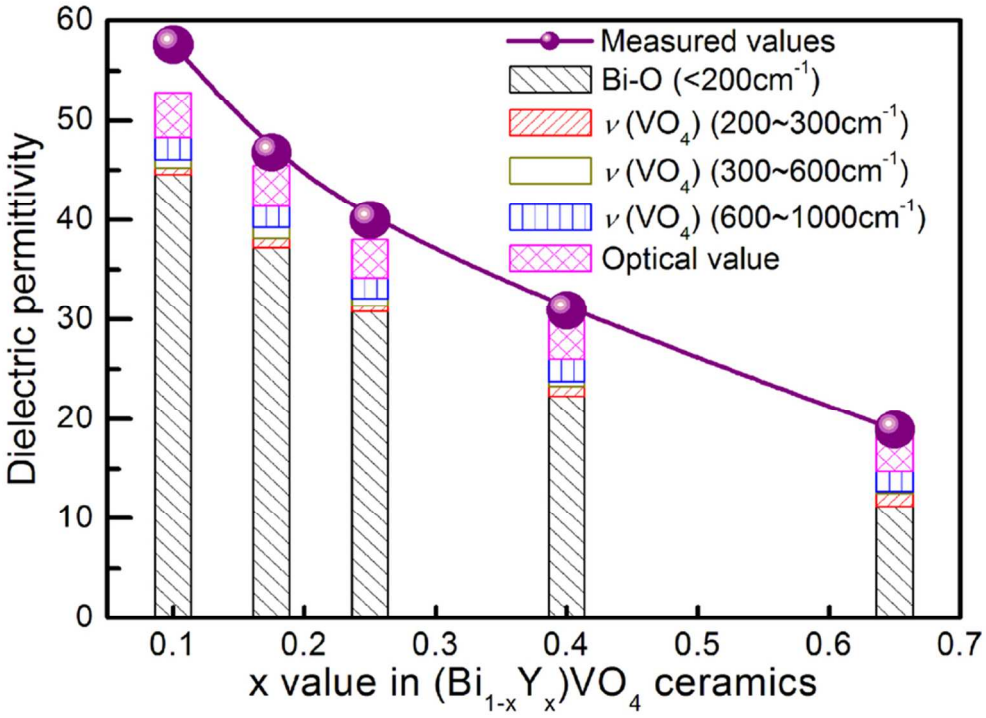

76x55mm (300 x 300 DPI)